Modulation of Spike-Mediated Synaptic Transmission by Presynaptic Background Ca^{2+} in Leech Heart Interneurons

Andrei I. Ivanov and Ronald L. Calabrese
Biology Department, Emory University, Atlanta, Georgia 30322

At the core of the rhythmically active leech heartbeat central pattern generator are pairs of mutually inhibitory interneurons. Synaptic transmission between these interneurons consists of spike-mediated and graded components, both of which wax and wane on a cycle-by-cycle basis. Low-threshold Ca^{2+} currents gate the graded component. Ca imaging experiments indicate that these low-threshold currents are widespread in the neurons and that they contribute to neuron-wide changes in internal background Ca^{2+} concentration (Ivanov and Calabrese, 2000). During normal rhythmic activity, background Ca^{2+} concentration oscillates, and thus graded synaptic transmission waxes and wanes as the neurons move from the depolarized to the inhibited phases of their activity.

Here we show that in addition to gating graded transmitter release, the background Ca^{2+} concentration changes evoked by low-threshold Ca^{2+} currents modulate spike-mediated synaptic transmission. We develop stimulation paradigms to simulate the changes in baseline membrane potential that accompany rhythmic bursting. Using Ca imaging and electrophysiological measurements, we show that the strength of spike-mediated synaptic transmission follows the changes in background Ca^{2+} concentration that these baseline potential changes evoke and that it does not depend on previous spike activity. Moreover, we show using internal EGTA and photo-release of caged Ca^{2+} and caged Ca^{2+} chelator that changes in internal Ca^{2+} concentration modulate spike-mediated synaptic transmission. Thus activity-dependent changes in background Ca^{2+}, which have been implicated in homeostatic regulation of intrinsic membrane currents and synaptic strength, may also regulate synaptic transmission in an immediate way to modulate synaptic strength cycle by cycle in rhythmically active networks.

Key words: **central pattern generator; leech heart interneurons; Ca currents; presynaptic background Ca^{2+}; synaptic transmission; short-term synaptic plasticity; photo-release of caged Ca^{2+}/Ca^{2+} chelator**

Introduction

Short-term modifications in synaptic strength on the basis of previous activity are a hallmark of neuronal networks that process sensory information and program motor outflow. In rhythmically active networks that form the core of central pattern generators, short-term synaptic modification has profound effects on patterned output and confers multistability that can be accessed by organizing synaptic input (Nadim et al., 1999).

Although it has been difficult to determine the precise mechanisms that underlie the different forms of short-term depression at synapses (Jiang and Abrams, 1998), various forms of short-term enhancement such as post-tetanic potentiation and facilitation appear to be caused presynaptically by the buildup of residual or background Ca^{2+}, which enhances vesicular release (Zucker, 1999). With the removal of presynaptic residual Ca^{2+}, short-term enhancement subsides. Thus, in rhythmically active networks, short-term synaptic enhancement based on activity-dependent increases in presynaptic residual Ca^{2+} provides a mechanism by which synaptic strength can be continuously modified on a cycle-by-cycle basis.

In the rhythmically active leech heartbeat central pattern generator, two segmental pairs of oscillator interneurons form mutual inhibitory synapses that ensure alternating bursting and show cycle-by-cycle waxing and waning in synaptic strength (Olsen and Calabrese, 1996).

Synaptic transmission between these interneurons consists of both spike-mediated and graded components. Spike-mediated synaptic strength depends on the membrane potential baseline from which a presynaptic spike arises and not on previous spike activity (Nicholls and Wallace, 1978a). The graded synaptic transmission depends on two low-threshold Ca^{2+} currents: one rapidly inactivating (I_{CaF}) and the other slowly inactivating (I_{CaS}) (Angstadt and Calabrese, 1991). Ca imaging experiments (Ivanov and Calabrese, 2000) indicate that these low-threshold currents are widespread in the neurons and that they contribute to neuron-wide changes in background Ca^{2+} concentration, whereas spikes produce no detectable widespread changes in Ca^{2+} concentration. During normal rhythmic activity, these widespread concentration changes wax and wane as the neurons move from the depolarized to the inhibited phases of their activity. Graded synaptic transmission is correlated with the widespread changes in background Ca^{2+} concentration brought on by these low-threshold currents.

Here we test the hypothesis that in addition to gating graded transmitter release, the presynaptic background Ca^{2+} concentration changes evoked by low-threshold Ca^{2+} currents modulate the strength of spike-mediated synaptic transmission. We develop stimulation paradigms to simulate the changes in baseline membrane potential that accompany rhythmic bursting. These

Received July 16, 2002; revised Nov. 18, 2002; accepted Nov. 21, 2002.

This work was supported by National Institutes of Health Grant NS24072. We thank Dr. Adam L. Weaver and Anne-Elise Tobin for their critical reading of this manuscript.

Correspondence should be addressed to Andrei I. Ivanov, Biology Department, Emory University, 1510 Clifton Road, Atlanta, GA 30322. E-mail: aivanov@biology.emory.edu.

 0270-6474/03/231206-13$15.00/0

stimuli evoke graded as well as spike-mediated postsynaptic responses and allowed us to explore the influence of background Ca^{2+} on each. Using Ca imaging and concurrent electrophysiological measurements, we show that the amplitude of spike-mediated postsynaptic responses follows the increases in background Ca^{2+} concentration that these baseline potential changes evoke. Experiments using internal EGTA and photo-release of caged Ca^{2+} and caged Ca^{2+} chelator show that increases in internal Ca^{2+} concentration evoke graded and enhance spike-mediated synaptic transmission. Activity-dependent changes in background Ca^{2+} concentration have been implicated in the homeostatic regulation of intrinsic membrane currents and potentially synaptic strength (Turrigiano, 1999); our results indicate that these changes in presynaptic background Ca^{2+} concentration may regulate synaptic transmission in an immediate way to modulate synaptic strength cycle by cycle in rhythmically active networks.

Materials and Methods

Animals. Adult leeches (*Hirudo medicinalis*) were obtained from Leeches USA and Biopharm and maintained in artificial pond water (Leeches USA) at ~15°C.

Preparation. Leeches were anesthetized in cold saline, after which individual ganglia (midbody ganglion 3 or 4) were dissected and pinned in a clear, Sylgard-coated open bath recording/imaging chamber (RC-26, Warner Instrument Corp.) with a 150 μl working volume. The sheath on the ventral surface of the ganglion was removed with microscalpels. Ganglia were superfused continually with normal leech saline (Nicholls and Baylor, 1968) containing (in mM): 115 NaCl, 4 KCl, 1.8 $CaCl_2$, 10 glucose, and 10 HEPES acid buffer, adjusted to pH 7.4 with NaOH or HCl. The preparation was mounted ventral side up (unless noted otherwise) on the stage of an Olympus BX50WI fluorescent microscope with an Olympus 40×/0.80 W water immersion objective.

Heart interneurons were identified by the posterolateral position of their somata on the ventral surface of the ganglion and by their characteristic pattern of rhythmic bursting. Once the heart interneurons in a ganglion were identified, one cell (presynaptic) was iontophoretically filled with the Ca^{2+}-sensitive fluorescent dye Calcium Orange, or with Calcium Orange in combination with either caged Ca^{2+} (NP-EGTA) or caged Ca^{2+} chelator (Diazo-2). In a small number of preliminary experiments, presynaptic cells were filled iontophoretically with the Ca^{2+}-sensitive fluorescent dye Fura-2. The opposite cell (postsynaptic) remained unfilled.

Calcium Orange [Molecular Probes, Calcium Orange, tetrapotassium salt "cell impermeant"; excitation/emission: 549/576; molecular weight (MW) 1087.33; catalog #C-3013] is a long-wavelength calcium indicator with a nominal K_d of 185 nM (at pH 7.2, 22°C) (Haugland, 2002). Eberhard and Erne (1991) measured a K_d of 434 nM at pH 7.2 and 457 at pH 7.4, a dissociation rate constant of 233 sec^{-1}, and an association rate constant of 0.51×10^9 $M^{-1}sec^{-1}$. The fluorescence of Calcium Orange increases linearly on its binding to Ca^{2+} in the range of free Ca^{2+} concentrations from 0.02 to at least 0.20 μM, with an approximately four- to fivefold increase from 0 to 39.8 μM free Ca^{2+} (Haugland, 2002).

Thomas et al. (2000) in experiments with HeLa cells, found that Calcium Orange has a rather small dynamic range, compared with Fluo-3, Calcium Green-1, and Oregon Green 488, and a prominent tendency to compartmentalization that makes it "the least useful indicator." In our preliminary experiments, Calcium Green-1, Oregon Green 488 BAPTA-1, and Fluo-3 did not show any remarkable advantages over Calcium Orange. Instead, use of Calcium Green-1 and Oregon Green 488 BAPTA-1 led to unacceptable background fluorescence, and all three indicators (especially Fluo-3) had a stronger tendency to photobleach than Calcium Orange [see also Thomas et al. (2000)].

NP-EGTA (Molecular Probes, *o*-nitrophenyl EGTA, NP-EGTA, tetrapotassium salt, "cell impermeant"; MW 653.81; catalog #N-6802) is a highly selective form of caged Ca^{2+}, releasing Ca^{2+} during UV illumination. NP-EGTA has a nominal K_d for Ca^{2+} before UV illumination of 80 nM and after illumination of 1 mM (Ellis-Davies and Kaplan, 1994), with a ratio of K_d for Ca^{2+} after illumination/before illumination of 1.2×10^4; NP-EGTA has a nominal K_d for Mg^{2+} of 9 mM, with a ratio of K_d for Mg^{2+} after illumination/before illumination of 1 (Nerbonne, 1996; Haugland, 2002).

Diazo-2 (Derived from BAPTA, "caged BAPTA"; Molecular Probes, Diazo-2, tetrapotassium salt, "cell impermeant"; MW 710.86; catalog #D-3034) is a photoactivatable Ca^{2+} scavenger; the nominal K_d of Diazo-2 for Ca^{2+} changes during UV illumination from 2.2 μM to ~80 nM (Adams and Tsien, 1993; Delaney, 2000). Both caged compounds used photo-release Ca^{2+}/Ca^{2+} chelator during UV illumination at <360nm.

Fura-2 (Molecular Probes, Fura-2, pentapotassium salt "cell impermeant"; MW 832.00; excitation: 340 and 380 nm, emission: 510 nm; catalog #F-1200) is a dual-wavelength calcium indicator with a nominal K_d of 145 nM (Haugland, 2002). To obtain K_d, R_{min}, R_{max}, F_{2free}, and F_{2bound}, we calibrated the Fura-2 signal *in vitro*, using the imaging setup, described in Intracellular Ca concentration evaluation, and a Calcium Calibration Kit with Mg^{2+} #2 (Molecular Probes; catalog #C-3722), which provides 11 prediluted buffers with mixes of K_2EGTA and CaEGTA, with free Ca^{2+} concentration from 0 to 39 μM, containing 1 mM free Mg^{2+}. We estimated the Fura-2 K_d for Ca^{2+} in the presence of 1 mM free Mg^{2+} to be 217 nM, which is close to the K_d of 224 nM provided by Grynkiewicz et al. (1985).

To fill cells with Calcium Orange or with Fura-2, heart interneurons were penetrated with thin-walled (1 mm outer diameter, 0.75 mm inner diameter) borosilicate microelectrodes (A-M Systems). The very tip of the electrode was filled with a solution of the desired indicator (5 mM solution in 300 mM K-acetate), and the rest of it was filled with 4 M K-acetate, 20 mM KCl (unbuffered, pH 8.4). To inject dye into the cells, a negative current of −1 nA (50% duty cycle) for 10–20 min was used. To fill cells with NP-EGTA or Diazo-2, the same techniques but different microelectrode solutions were used. To fill cells with NP-EGTA, the solution contained (in mM): 5 Calcium Orange, 40 NP-EGTA, 32 $CaCl_2$, 40 KOH/HEPES, pH 7.2. To fill cells with Diazo-2, the solution contained (in mM): 5 Calcium Orange, 40 Diazo-2, 40 KOH/HEPES, pH 7.2.

Electrophysiology. Recording microelectrodes filled with 4 M K-acetate, 20 mM KCl (unbuffered, pH 8.4) of the same kind as used for dye injection were inserted into both cells 5–15 min after the cells were filled with dye or caged compounds or both. In some experiments, noted in Results, the microelectrode used for recording from the presynaptic cell contained additionally 0.2 M EGTA, the slow Ca chelator. Microelectrodes were coated along their shanks with Sylgard 186 (Dow-Corning) and had resistances of 20–45 MΩ and time constants of 0.5–1.5 msec when capacity was compensated.

Once the cells were penetrated with recording microelectrodes, the superfusate was switched to a high Mg^{2+}/high Ca^{2+} saline that contained (in mM): 80.5 NaCl, 4.0 KCl, 5.0 $CaCl_2$, 20 $MgCl_2$, 10.0 glucose, 10.0 HEPES acid buffer, adjusted to pH 7.4 with KOH or HCl. This elevated divalent ion solution effectively suppresses spontaneous spike activity in heart interneurons but does not markedly affect their synaptic transmission (Nichols and Wallace, 1978a).

In all experiments, the activity of the presynaptic cell was recorded in current-clamp mode, whereas the activity of the postsynaptic cell was recorded either in current-clamp mode or in voltage-clamp mode. Voltage-clamp recordings were made with an Axoclamp-2A amplifier (Axon Instruments, Foster City, CA) in single-electrode voltage-clamp mode with a sampling rate of 2.5 or 5 kHz. Current-clamp recordings were made with an Axoclamp-2A amplifier used in discontinuous current-clamp mode with a sampling rate of 2.5 or 5 kHz. In each case, the electrode potential was monitored on an oscilloscope to ensure that the potential settled between current injection cycles. All recordings were referenced to a chlorided silver wire used to ground the bath. All electrophysiological data were acquired, digitized, and stored on a Pentium or Pentium II (Intel) computer using pCLAMP 7.0/8.0 software with a Digidata 1200 or 1320A interface from Axon Instruments.

All stimulus protocols were generated using the pCLAMP program CLAMPEX. During normal rhythmic activity (period of ~6–10 sec), oscillator heart interneurons move from a potential of approximately

−55 mV during their inhibited phase to a burst phase during which the spikes appear to arise from a potential of approximately −45 mV (Hill et al., 2001). The elevated divalent cation concentration of the bathing solution used in these experiments (5 mM Ca^{2+}, 20 mM Mg^{2+}) raised the threshold for spiking in the interneurons to above −40 mV and suppressed rhythmic activity. To simulate normal excursions in membrane potential, we developed a depolarizing step protocol. The usual protocol mimicked the depolarized burst phase of the presynaptic cell by a 2 sec current step to a potential of approximately −40 mV, from and back to a holding potential of −50 to −65 mV. During this current step, either a train of brief (6 msec) suprathreshold current pulses was superimposed or individual suprathreshold current pulses were superimposed at various times (usually at 36, 422, 808, 1194, 1580, and 1966 msec from the beginning of the depolarizing step). The trains of current pulses were generated by an S48K Square pulse stimulator (Astro-Med, Grass Instrument Division) that was triggered by CLAMPEX and in turn gated the constant current source of the Axoclamp-2. In some experiments, suprathreshold pulses were applied before and after the depolarizing step. In some cases, the brief suprathreshold pulses were applied without the long subthreshold depolarizing current. The postsynaptic cell was typically held at approximately −40 mV in voltage clamp or by current injection in current clamp.

Ca imaging. Changes in Calcium Orange fluorescence were monitored continuously and recorded with an ICCD-350f CCD camera (Video Scope International) connected to the fluorescent microscope mentioned above, equipped with an Olympus U-MNG (exciter filter BP 530–550 nm, dichroic mirror DM 570 nm, barrier filter BA 590 nm) filter set, 10% neutral density filter, and Olympus 40×/0.80 W water immersion objective and Axon Imaging Workbench 2.1/2.2/4.0 software with a Digidata 2000 interface (Axon Instruments) on a Pentium II (Intel) computer. Intensifier gain and black (baseline) levels were adjusted to achieve minimal background fluorescence, convenient visualization of the filled neuron, and sufficient dynamic range for monitoring fluorescence changes.

Our setup permits the acquisition of full-frame images of 640 × 480 pixels at a resolution of 0.379 μm^2 for 1 pixel (395 × 295 μm for full frame) with the Olympus 40×/0.80 W water immersion objective. Changes of fluorescence were recorded from one or more zones, which are numbered in Figure 1*B*. Zones 1–3 were 20–60 pixels (7.58–22.74 μm^2) and corresponded to single neuritic branches, and zone 4 was 600–1200 pixels (235–470 μm^2) and corresponded to the approximate synaptic contact region of a heart interneuron. Only those parts of interneurons in which the fluorescence measurement remained unsaturated during the entire experimental protocol were used to monitor changes of fluorescence. In all experiments, the maximal available acquisition rate (video rate, 30 Hz) was used, yielding a time resolution of 33 msec. Video signals were accumulated for 33 msec per image, without any kind of gating, using the DC mode of the camera.

To synchronize the acquisition of electrophysiological data and Ca fluorescence recording, the Digidata 2000 and Digidata 1200/1320A were connected using a DIO-3 cable interface (Axon Instruments) that permits one program to trigger the other. In our experiments, we used pCLAMP 7.0/8.0 protocols to trigger data acquisition by Axon Imaging Workbench, which in turn controlled the shutter for the imaging lamp.

Stored data were analyzed on the same computer using pCLAMP program CLAMPFIT, Microcal Origin 6.1 and StatSoft Statistica software. Illustrations were created using Adobe Photoshop 6.0 and Adobe Illustrator 10.0 software. Calcium fluorescence data are presented mainly as changes in fluorescence ($\Delta F/F$), but in some cases as fluorescence (F); in this latter case (see Fig. 2), the data are presented in units of absolute fluorescence on a scale from 0 to 255 fluorescence units. Results of statistical analysis are presented/plotted as mean ± SE.

Intracellular Ca concentration evaluation. Fluorescence of Fura-2 was recorded using basically the same setup as above but equipped with filter set XF04 (Omega Optical), which included exciter filters 340HT15 (center wavelength 340 nm) and 380HT15 (center wavelength 380 nm), dichroic mirror 430DCLP02 (cutoff wavelength 430 nm), emitter filter 510WB40 (center wavelength 510 nm), and a 25% neutral density filter. All other details of the setup were the same.

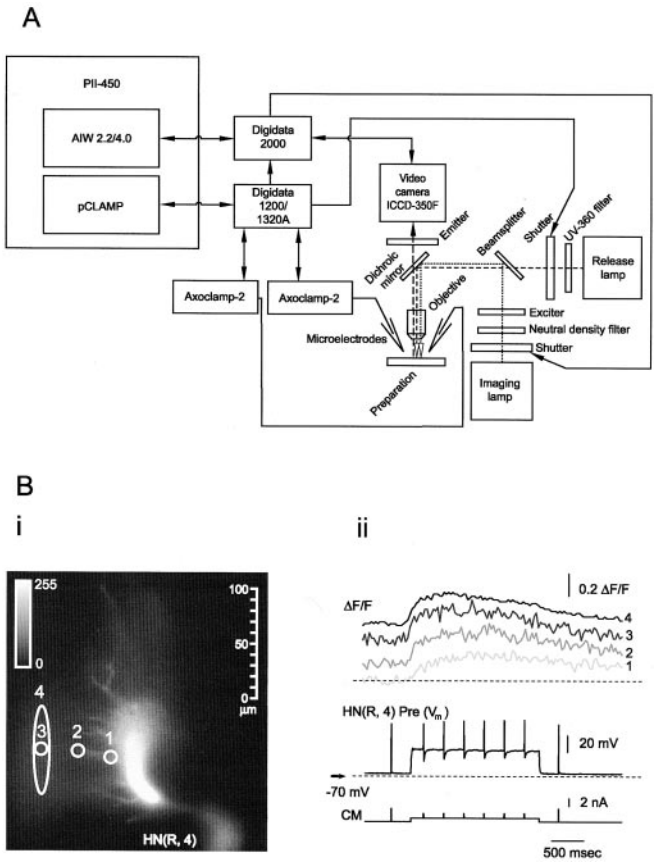

Figure 1. *A*, Schematic of experimental setup. *Lines* with *arrowheads* indicate control communication lines and their direction. *Dotted* and *dashed lines* indicate light paths and beams, and *lines* ending in *electrode symbols* are electrical connections. *B*, Simultaneous recordings (*ii*) of electrophysiological activity and Ca fluorescence changes ($\Delta F/F$) in fine branches. The preparation was mounted dorsal side up to image fine branches (*i*). A step depolarization (stimulus protocol used in several of the experiments reported) of the imaged cell led to a widespread change in Ca fluorescence recorded at the numbered *circles*/*oval*. Note that the fluorescence signal recorded in the *oval* (*4*), which covers a large portion of the synaptic contact region, is very similar to that recorded in a much more restricted portion of the synaptic contact region (*3*) but is less noisy. The fluorescence signal recorded near the main neurite (*1*) rises and falls more slowly than in the synaptic contact region (*3*, *4*). In this and all subsequent images, the location and relative size of the fluorescence recording sites are indicated, but they are exaggerated in size for legibility, and in all images presented the intensity of fluorescence is coded by a *linear gray*/*pseudocolor scale inset* (*0–255*). In this and subsequent figures, membrane potential recordings (V_m) of heart interneurons are labeled *HN* and indexed by body side and ganglion number of the recorded cell. V_m records labeled *Pre* were from cells that were stimulated and thus functionally presynaptic. In each case, their Ca fluorescence signals were recorded synchronized with the voltage recordings. The current monitor trace for the *Pre* cell is labeled *CM*. In all the experiments illustrated in subsequent figures, postsynaptic responses to the *Pre* cell stimulation were recorded in the opposite (Post) heart interneuron in voltage clamp (IPSC) or current clamp (IPSP).

In these experiments only one cell was recorded. Cells were held at different holding potentials for not less than 60 sec, after which the emission at 510 nm for excitation at 340 nm and at 380 nm each was recorded for 10 sec. The signal was acquired from zone 4 (see above). For background subtraction the nearest region with little change in fluorescence was used. The concentration of free intracellular Ca^{2+} was calculated as $[Ca^{2+}]_i = K_d \times (F_{2free}/F_{2bound}) \times (R - R_{min})/(R_{max} - R)$ (Grynkiewicz et al., 1985), using parameters obtained during the *in vitro* calibration.

UV photolysis of caged Ca^{2+}/Ca^{2+} chelator. For experiments of this kind, the optical system was modified (Fig. 1*A*). A 100 W mercury lamp (release lamp), equipped with a UV transmitting fused-silica condenser, an electronic shutter (Oriel Instruments), and a glass UV filter (U-360, Edmunds Industrial Optics), was connected by a UV transmitting fused-

silica fiber (core diameter 1000 μm, numerical aperture 0.22; Oriel Instruments) to an "ablation laser unit" (Photonic Instruments) that was attached to the microscope. To make the connection, the resonator block of the ablation laser unit was removed, and the fiber, equipped with a UV-transmitting fused-silica focusing beam probe (Oriel Instruments), was connected to the port of the resonator block. A second 100 W mercury lamp (imaging lamp), used for fluorescent imaging, was attached to a lamp-house block of the ablation laser unit. The UV-transmitting 50/50 beam splitter permitted us to deliver the light of both mercury lamps through the optical system of the microscope to the preparation, making it possible to monitor and record Ca fluorescence and to photo-release caged compounds simultaneously. In some of these experiments, we used the filter set described above. In others we used exciter filter XF1074 (525AF45, center wavelength 525 nm), dichroic mirror XF2032 (565DRLPXR, cutoff wavelength 565 nm), and emitter filter XF3083 (595AF60, center wavelength 595 nm) from Omega Optical. In each case, the exciter was installed not in the microscope's standard filter cube, but between the imaging lamp and the lamp-house block of the ablation laser unit. The location and focusing of the spot of "uncaging" light were adjusted with controls on the ablation laser unit so that the spot was centered in the image plane. To estimate the area of effective uncaging of our light spot, a water–glycerol solution of 4,5-dimethoxy-2-nitrobenzyl (DMNB)-caged fluorescein (~100 μM) (Molecular Probes, DMNB-caged fluorescein dextran anionic; MW 3000; catalog #D-3309) was placed on a slide under a coverslip, and the ability of the system to uncage the fluorescein was tested (Wang and Augustine, 1995; Parpura and Haydon, 1999). The intensity (neutral density filter) and diameter (iris diaphragm) of the spot were then adjusted so that fluorescein was uncaged in an area of 7400 pixels (2800 μm^2) (see Figs. 8, 11), as measured from the first image, acquired after and during fluorescein uncaging. Lateral diffusion of uncaged fluorescein in the water–glycerol solution was rather slow, so our method provided a reasonable estimate of the area of uncaging. Similar values were obtained by measuring the area and diameter of the light spot, focused on green paper.

All protocols used for photo-release of caged compounds were generated using the pCLAMP program CLAMPEX, which controlled the shutter of the release lamp through the Digidata 1200/1320A connected to the shutter control unit. Typically, Ca^{2+}/Ca^{2+} chelators were photo-released for 200–800 msec during electrophysiological and Ca fluorescence data acquisition.

Results

Changes in presynaptic background Ca^{2+} can account for the modulation of spike-mediated synaptic transmission between heart interneurons by membrane potential

During normal activity, heart interneurons burst rhythmically, moving from an inhibited phase (approximately −55 mV) to a burst phase (approximately −40 mV at the base of the action potentials). The average burst period is ~6–10 sec, and average spike frequency during a burst is ~12 Hz (Hill et al., 2001). The amplitude of spike-mediated IPSCs varies smoothly with presynaptic membrane (slow wave) potential as activity moves between these phases (Nicholls and Wallace, 1978a; Olsen and Calabrese, 1996). The general hypothesis, first put forth by Nicholls and Wallace (1978a), that we wanted to test was that level of background Ca^{2+} in the neuron modulates the amplitude of spike-mediated synaptic transmission and thus accounts at least in part for the effect of membrane potential. Our previous results (Ivanov and Calabrese, 2000) had indicated that Ca^{2+} entry through low-threshold Ca channels determines this background level of Ca^{2+} throughout the neuron. All experiments reported here were performed in 20 mM Mg^{2+}/5 mM Ca^{2+} saline, which blocks all spontaneous activity in heart interneurons (see Material and Methods). This solution has been used successfully to study the effect of membrane potential on spike-meditated synaptic transmission (Nicholls and Wallace, 1978a).

Figure 2 illustrates this phenomenon under steady-state conditions; the average amplitude of spike-mediated IPSCs (smIPSCs) evoked by single spikes in heart interneurons follows membrane potential over the range −50 to −35 mV and saturates at more depolarized potentials. Background Ca fluorescence, throughout the entire neuritic tree, increases over the same range and shows similar saturation. IPSC amplitude and background Ca fluorescence are well correlated ($r = 0.98$; $p < 0.005$). At each baseline membrane potential, we observed stochastic variation in IPSC amplitude but no tendency for amplitude to vary systematically with spike number in our simulated bursts. Similar results were obtained in three other preparations. Although spike amplitude varied somewhat in these experiments, no relationship between spike amplitude and smIPSC amplitude was apparent. In a few cells ($n = 4$), we estimated the concentration of free intracellular Ca^{2+} at −70 and −35 mV using the two-wavelength indicator dye Fura-2 under similar conditions. Our results indicate a $[Ca^{2+}]_i$ of 61.0 ± 12.9 nM at −70 mV and 86.7 ± 10.1 nM at −35 mV.

To approximate the changes in the slow wave of presynaptic membrane potential during a normal burst, we developed stimulation protocols in which the membrane potential was stepped between a hyperpolarized level (−70 to −50 mV) and a depolarized (but subthreshold because of the increased divalent cations in the saline) level (−45 to −35 mV) with a current step (2–6 sec). Individual spikes were evoked by short current pulses superimposed on this changing background potential. Figure 3*A* illustrates such a simulated burst and demonstrates that smIPSC amplitude first dramatically increases and then decreases toward a steady state during the 6 sec time course. The change in presynaptic Ca fluorescence follows a similar time course. There is also prominent graded synaptic transmission, seen as a slowly changing postsynaptic current (gIPSC), which rises and declines during the simulated burst. In Figure 3*B*, individual spikes were evoked from a steady baseline potential. At the beginning of the simulated burst, spikes evoked small stochastically varying smIPSCs, but later the current pulses used to evoke spikes elicited small Ca plateaus that were terminated when the next pulse evoked a spike (three similar preparations were recorded). The plateaus evoked large increases in presynaptic Ca fluorescence, and smIPSCs were greatly enhanced. These observations indicated that changes in presynaptic background Ca^{2+} may account for the modulation of smIPSP amplitude and its time course during slow-wave changes in presynaptic membrane potential.

Comparison of the time course of changes in spike-mediated synaptic transmission and background Ca fluorescence during step changes in membrane potential

We wished to determine the time course of changes in spike-mediated synaptic transmission during step changes in membrane potential in the absence of effects caused by the history of spike activity. Single presynaptic spikes were superimposed on long depolarizing steps (2 sec) at various times (one individual spike per long depolarizing step) and, in addition, in some experiments before and after the steps. Postsynaptic responses were monitored in either current clamp ($n = 16$) or voltage clamp ($n = 7$) as smIPSPs or smIPSCs, respectively. The results of three such experiments are illustrated in Figure 4*A–C*. As expected, the depolarizing steps evoked large increases in presynaptic Ca fluorescence recorded near the main neurite, like site 1 in Figure 1. These changes in fluorescence rose and then began to fall slowly during the step. The amplitude of the spike-mediated postsynaptic responses (smIPSPs or smIPSCs) increased and decreased during the step with a similar time course. There were no changes

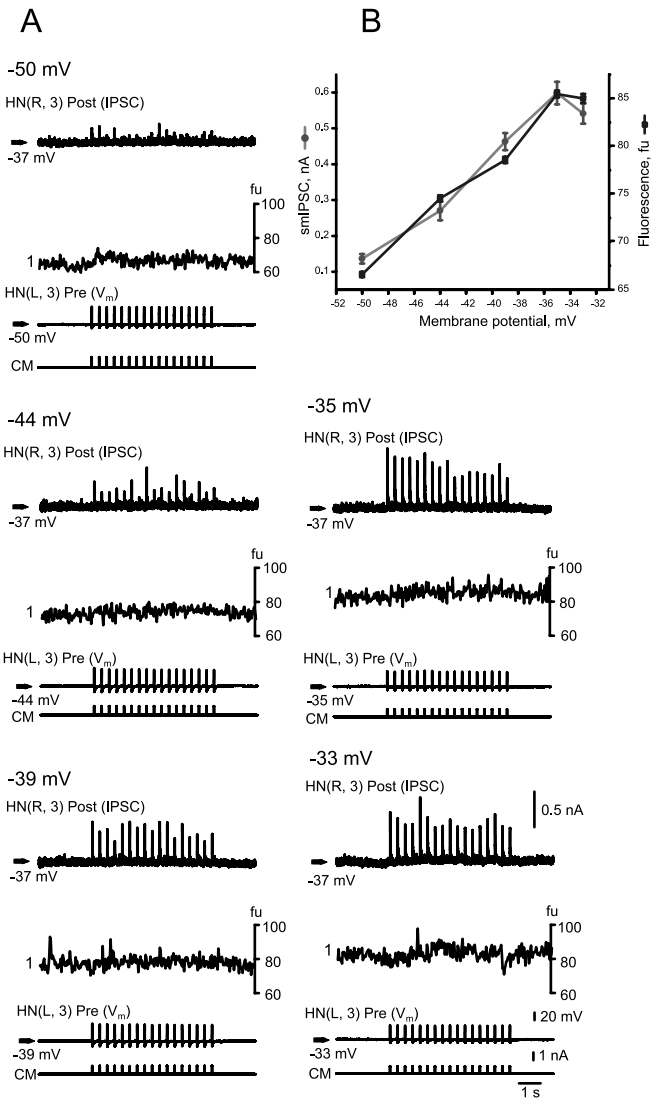

Figure 2. The amplitude of spike-mediated postsynaptic responses and the level of presynaptic background $[Ca^{2+}]_i$ both increase with the presynaptic holding potential. *A*, Spikes were evoked at five different holding potentials (−50, −44, −39, −35, and −33 mV) while we simultaneously recorded (near the main neurite) the presynaptic level of background Ca fluorescence, presented in units of absolute fluorescence (0–255 fu), and spike-mediated IPSCs. *B*, Graph showing the relations of average spike-mediated IPSC (*smIPSC*) amplitude and Ca fluorescence with presynaptic holding potential. In this and in all subsequent figures, data are plotted as mean ± SE. All of the recordings are from the same preparation.

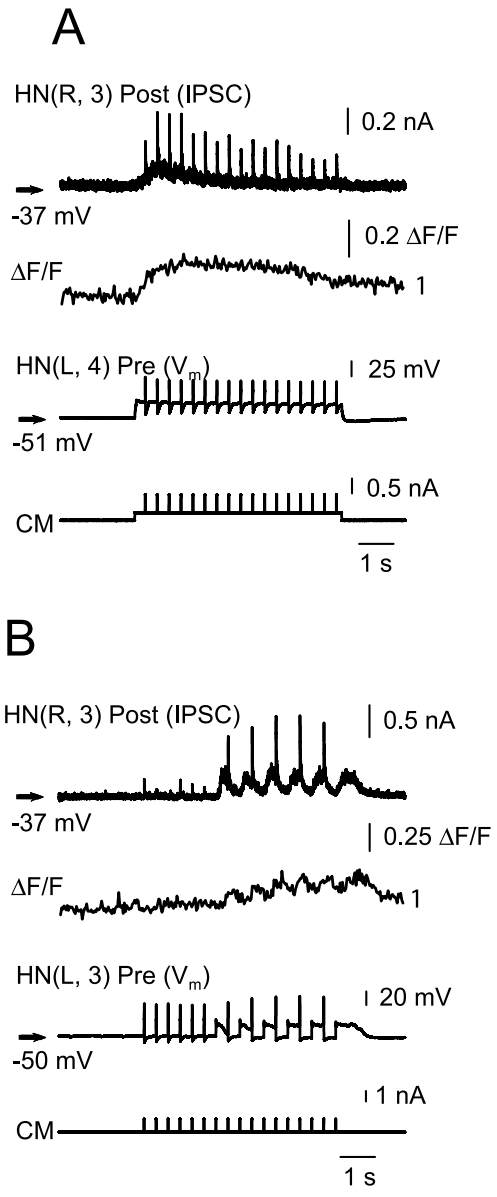

Figure 3. *A*, A simulated burst with underlying depolarization (spikes are superimposed on a step depolarization) produces an increase in Ca fluorescence ($\Delta F/F$), graded synaptic transmission, and modulation of spike-mediated transmission. Spike-mediated IPSCs increase and then decrease during the simulated burst. *B*, A simulated burst without underlying depolarization (spikes superimposed on a steady holding potential) in an unusual preparation. See Results for further explanation. *A* and *B* show recordings from different preparations.

in Ca fluorescence associated with evoked spikes. The amplitude of the spike-mediated postsynaptic responses did not depend on the amplitude of presynaptic action potential or on the magnitude of graded postsynaptic response, which in some preparations was negligible (Fig. 4*B*).

The amplitude of the postsynaptic responses appeared to depend only on when a presynaptic spike was evoked during the depolarizing step, and it followed a time course similar to evoked changes in Ca fluorescence (Fig. 4*D*,*E*). The time constants for a single exponential fit to the rise of the Ca fluorescence change and the amplitude of the postsynaptic responses were similar. Using a similar stimulus protocol, Nicholls and Wallace (1978a) measured a time constant of ~900 msec for the rise in the amplitude of spike-mediated IPSPs in response to a step depolarization. There was a strong correlation (smIPSPs, $r = 0.99$, $p < 0.005$; smIPSCs, $r = 0.99$, $p < 0.005$) between the amplitude of the postsynaptic responses and the change in presynaptic Ca fluorescence.

Although in the previous experiments Ca fluorescence was recorded near the main neurite, in subsequent experiments we additionally recorded Ca fluorescence in fine neuritic branches and in the region of synaptic contacts between heart interneurons as described in Materials and Methods (Fig. 1*B*). Under the conditions of these experiments, Ca fluorescence changes evoked by depolarizing steps rise and fall more rapidly in the synaptic region than in the main neurite. Thus we were able to more precisely define the time course of changes in background Ca^{2+} in the presynaptic terminals. We also modified our stimulation protocol so that a series of spikes were evoked during each depolarizing

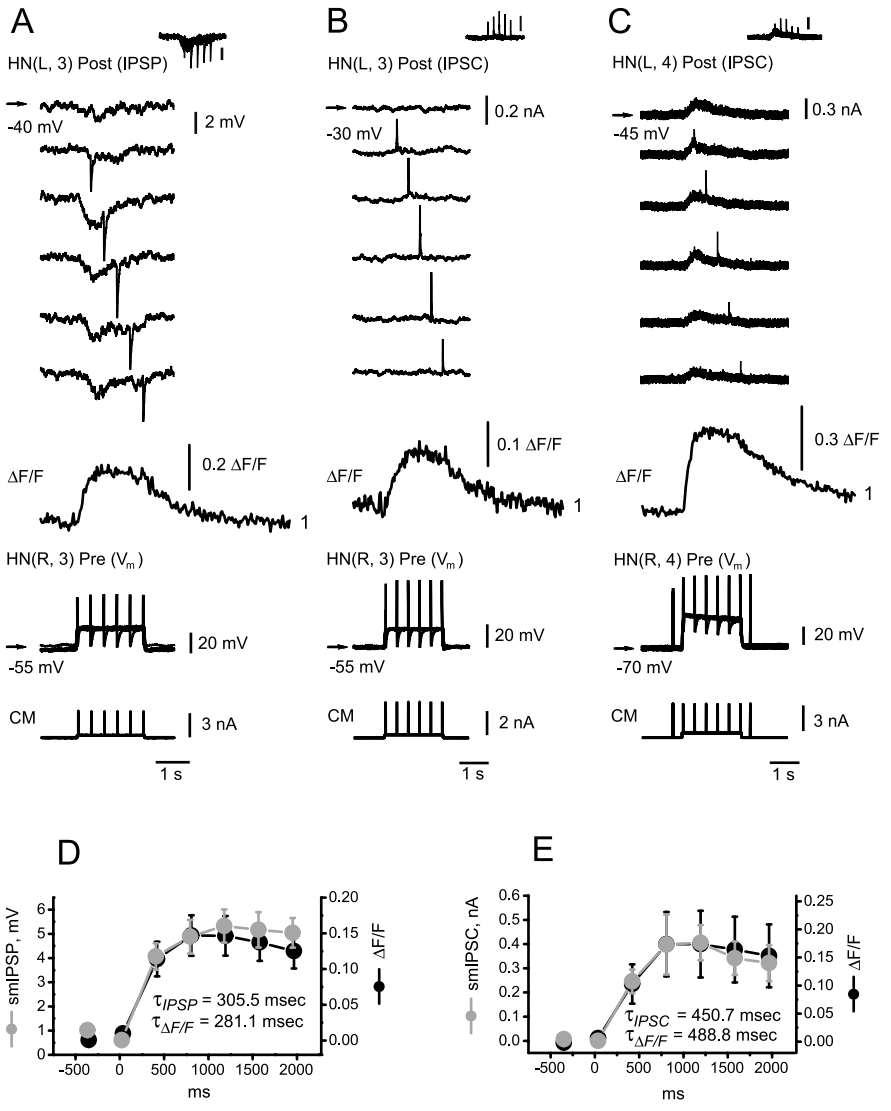

Figure 4. Plasticity in spike-mediated synaptic transmission evoked by a step depolarization follows the time course of changes in Ca florescence measured near the main neurite and is independent of previous spike activity. *A–C*, Single spikes were superimposed on a step depolarization at different times. Presynaptic recordings were superimposed, and Ca fluorescence ($\Delta F/F$) signals were averaged. Postsynaptic responses are presented as individual traces (see *insets* for superimposed responses). *A* illustrates experiments in which IPSPs were recorded ($n = 16$), and *B* and *C* illustrate experiments ($n = 7$) in which IPSCs were recorded. In *B* no graded IPSC was recorded, but spike-mediated plasticity followed a similar time course as when a graded IPSC was recorded as in *C*. *D*, *E*, Spike-mediated postsynaptic responses (*smIPSP* in *D* and *smIPSC* in *E*) and the change in the Ca fluorescence signal ($\Delta F/F$), averaged across experiments, are plotted versus the timing of the evoked spike from the start of the step depolarization. In some experiments (7 for recorded IPSPs and 5 for recorded IPSCs), a spike was evoked before the step depolarization as in *C*. A single exponential time constant was fitted to the rise of the postsynaptic responses (τ_{IPSP}/τ_{IPSC}) and the Ca fluorescence signal ($\tau_{\Delta F/F}$) in *D* and *E* using $f(t) = A_i e^{-t/\tau_i} + C$. *A* and *B* show recordings from the same preparation, and *C* shows recordings from a different preparation.

step to approximate more closely natural bursts and to allow us to proceed more rapidly in our experiments. Figure 5, *A* and *B*, illustrates two such experiments ($n > 25$ each for postsynaptic current clamp and postsynaptic voltage clamp). The time course of changes in postsynaptic responses during the step (Fig. 6*A1*,*A2*) was similar to the previous experiments in which only a single spike was evoked during each step (Fig. 4*D*,*E*). There was a close correspondence between the time course of changes in presynaptic Ca fluorescence recorded near the main neurite and spike-mediated postsynaptic responses (Fig. 6*B1a*,*B2a*) that was similar to the previous experiments. This close correspondence was not observed for Ca fluorescence changes in the synaptic region (Fig. 6*A1*,*A2*). Therefore, if changes in background Ca^{2+} in the presynaptic terminals are causally related to the modulation of postsynaptic responses, then binding and unbinding of Ca^{2+} at an important modulatory site may be rate limiting, or some slow process may follow this binding before modulation occurs. For example, the modulatory Ca^{2+} binding site, possibly a mobile buffer, may have high affinity and slow kinetics, or the consequences of Ca^{2+} binding at the modulatory site may involve a slow process such as vesicle mobilization (cf. Blundon et al., 1993; Winslow et al., 1994; Neher, 1998).

The effect of the slow Ca^{2+} chelator EGTA on the modulation of spike-mediated transmission by membrane potential

To test directly the dependence of synaptic modulation on background Ca^{2+}, we sought to reduce and delay the buildup of changes in background Ca^{2+} in the presynaptic terminals by introduction of EGTA presynaptically ($n > 15$ each for postsynaptic current clamp and postsynaptic voltage clamp). The experiments of Figure 5, *A* and *B*, served as controls for these experiments. Diffusion of EGTA from the recording microelectrode (200 mM) dramatically reduces both background Ca fluorescence and changes in Ca fluorescence associated with step depolarizations. Nevertheless, we were able to detect changes in Ca fluorescence in response to step depolarizations, particularly in the synaptic contact region. Figure 5, *C* and *D*, shows the effect of EGTA on presynaptic Ca fluorescence and postsynaptic responses using the same simulated burst protocol as in the experiments of Figure 5, *A* and *B*. Even in the absence of a detectable change in Ca fluorescence, the step depolarization evoked a strong increase in spike-mediated synaptic transmission and strong graded synaptic transmission. Intracellular EGTA slows the buildup of spike-mediated synaptic transmission and slightly reduces its amplitude compared with control conditions (Fig. 5, compare *A*, *B* with *C*, *D*.). The time constants of buildup of synaptic plasticity increased with respect to control, and the time constants of Ca fluorescence buildup in the synaptic contact region were correspondingly increased (Fig. 6*B*). Regression analysis (Fig. 5*E*,*F*) showed a significant linear relationship between the amplitude of the Ca fluorescence signal in the synaptic contact region and the amplitude of the postsynaptic response (smIPSP $= -0.817 + 189.17 \times \Delta F/F$, $r^2 = 0.96$, $p < 0.005$; smIPSC $= 0.054 + 2.523 \times \Delta F/F$, $r^2 = 0.97$, $p < 0.005$) in the presence of internal EGTA but not under control conditions. We conclude that when the buildup of background Ca^{2+} in the presynaptic terminals is delayed and reduced by EGTA, the back-

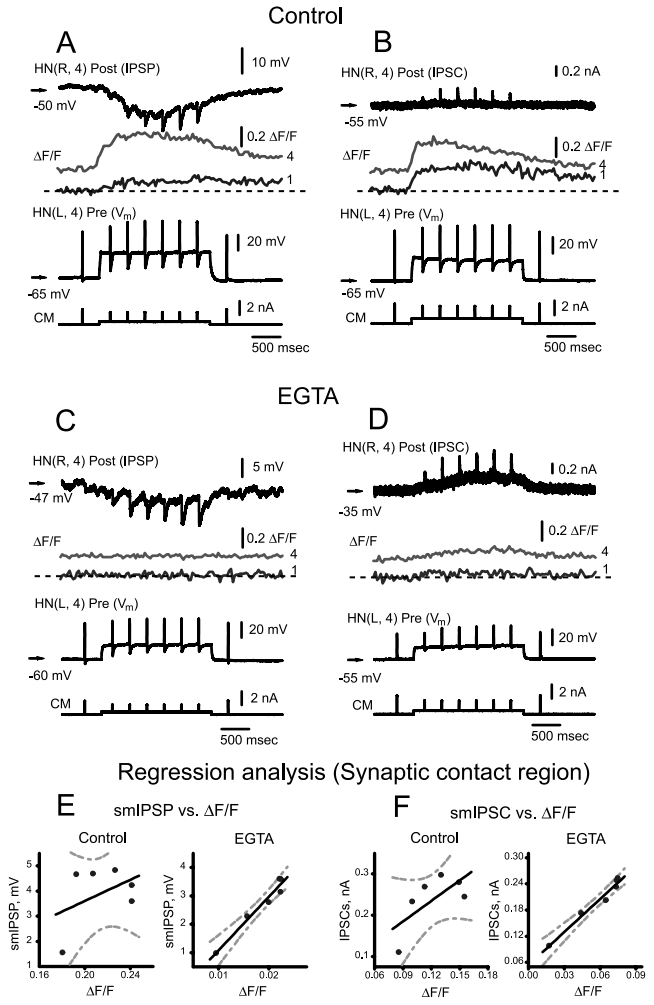

Figure 5. Plasticity in spike-mediated synaptic transmission evoked by a step depolarization (simulated burst protocol) compared with changes in Ca fluorescence. Ca fluorescence ($\Delta F/F$) was measured at two sites corresponding to the *numbered areas* in Figure 1*B*. Postsynaptic responses were measured as IPSPs (*A*, *C*) or IPSCs (*B*, *D*). *E*, *F*, Regression analysis of the spike-mediated postsynaptic responses (*E, smIPSP*; *F*, *smIPSC*) versus Ca fluorescence ($\Delta F/F$) in the synaptic contact region (*4*) averaged across experiments shows significant linear dependence only in the presence of internal EGTA. *Black lines* represent the best fit from a linear regression; *gray dotted lines* are 95% confidence intervals. In *A–D,* all of the recordings are from different preparations.

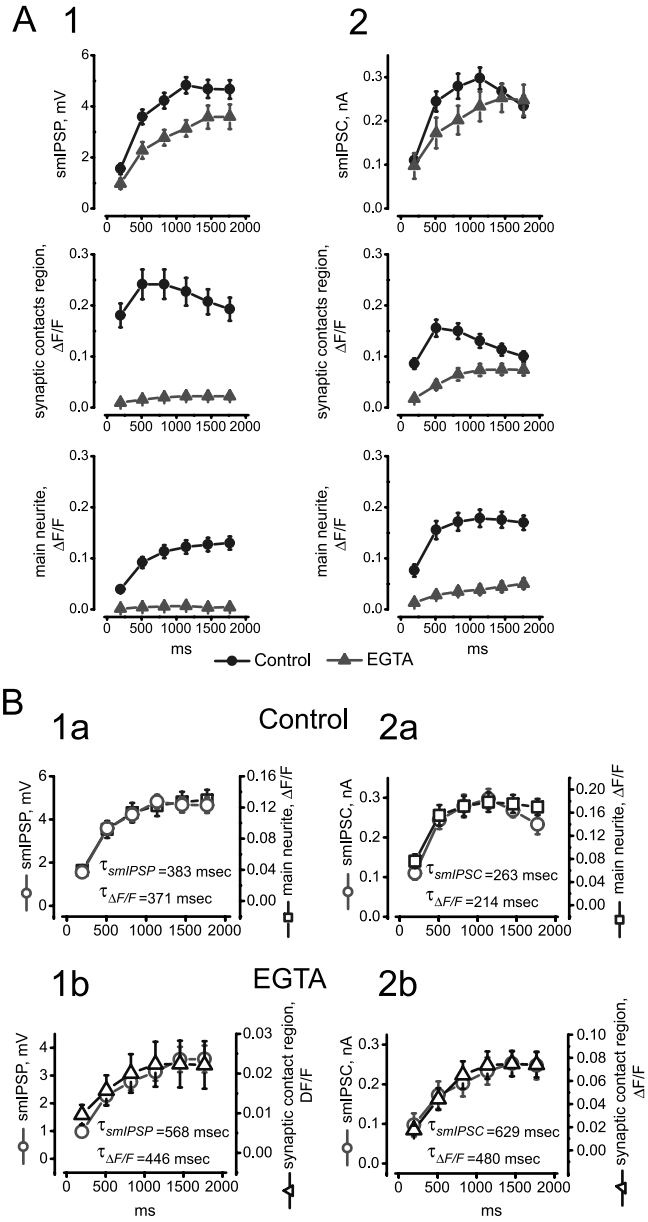

Figure 6. The time course of plasticity in spike-mediated synaptic transmission evoked by a step depolarization (simulated burst protocol) compared with the time course of changes in Ca fluorescence, under control conditions and in the presence of internal EGTA. Data are from the experiments illustrated in Figure 5. Changes in Ca florescence ($\Delta F/F$) were measured in the main neurite and synaptic contact region corresponding to sites *1* and *4* of Figure 1*B*. Postsynaptic responses were measured as smIPSPs (*1*) or smIPSCs (*2*). *A*, Comparison of spike-mediated postsynaptic responses (*1, smIPSP*; *2*, *smIPSC*) and Ca fluorescence changes ($\Delta F/F$) averaged across experiments under control conditions and in the presence of internal EGTA. *B*, Spike-mediated postsynaptic responses (*smIPSP* in *1* and *smIPSC* in *2*) and the change in the Ca fluorescence signal, averaged across experiments, are plotted versus the timing of the evoked spike from the start of the step depolarization under control conditions and in the presence of internal EGTA. A single exponential time constant was fitted to the rise of the postsynaptic responses (τ_{IPSP}/τ_{IPSC}) and the Ca fluorescence signal ($\tau_{\Delta F/F}$) in *1* and *2* in the main neurite (*a*) and the synaptic contact region (*b*) using $f(t) = A_1 e^{-t/\tau_1} + C$. Data presented here are from *A*.

ground Ca^{2+} concentration appears to be rate limiting for synaptic modulation. Although spike amplitude varied somewhat in these experiments and in other experiments using the simulated burst protocol, no relation between spike amplitude and smIPSC amplitude was apparent.

EGTA also had a dramatic effect on the time course but not on the amplitude or the integral of the graded postsynaptic response (Fig. 7). In the presence of internal EGTA, the integrated gIPSC was 95% of control. Under control conditions the time course of the rise in graded transmission and the time course of the buildup in Ca fluorescence in the synaptic contact region match closely (Fig. 7*B*, *Control*). This result is expected on the basis of our previous analysis of graded synaptic transmission (Ivanov and Calabrese, 2000). In the presence of internal EGTA, this similarity in time course is preserved: both buildup in the Ca fluorescence signal and the rise in graded transmission are delayed (Fig. 7*B*, *EGTA*). The difference in time courses for the rise in graded transmission and the modulation in spike-mediated transmission under control conditions suggests that these two processes involve different Ca-dependent mechanisms. The buildup of background Ca^{2+} in the presynaptic terminals appears to be rate limiting for graded transmission but not for the modulation in spike-mediated transmission.

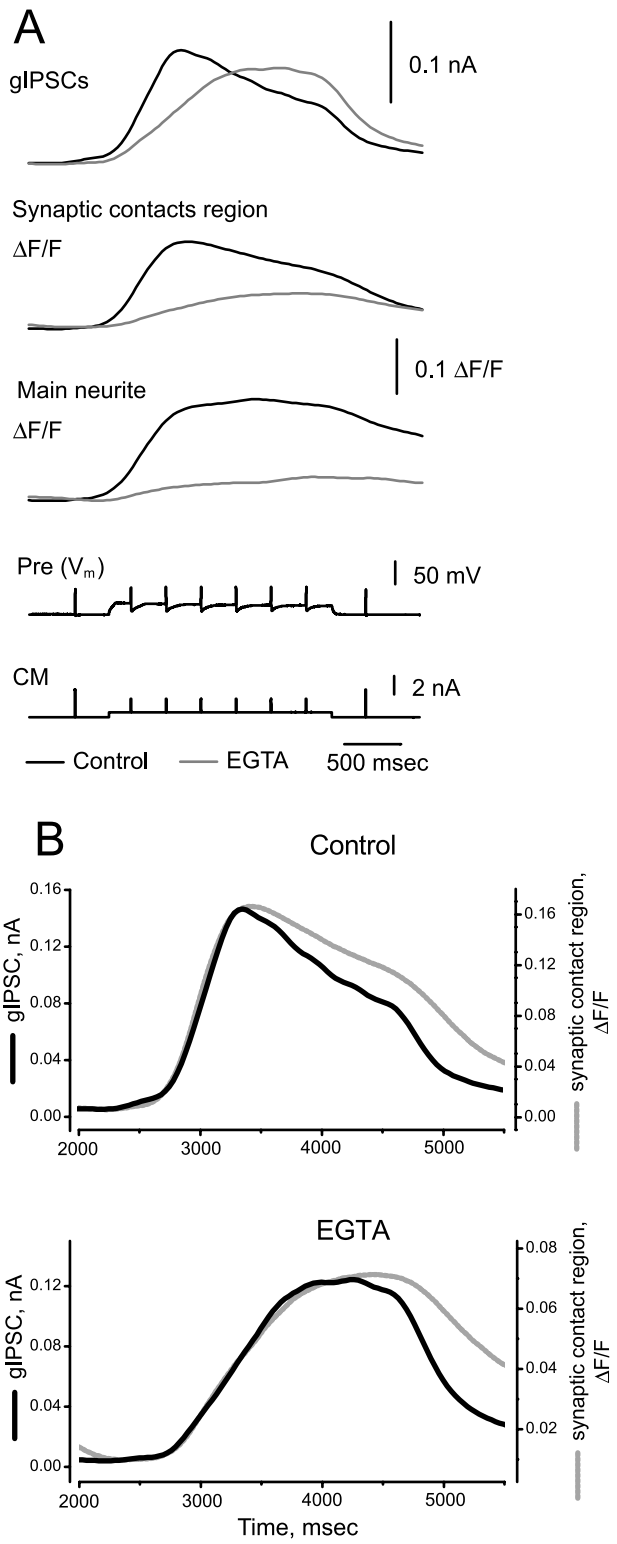

Figure 7. *A*, The time course of graded synaptic transmission (measured as gIPSC) evoked by a step depolarization (simulated burst protocol) compared with the time course of changes in Ca florescence, under control conditions and with internal EGTA. Data are averages from the experiments illustrated in Figure 5. In this and subsequent figures, gIPSCs were obtained by low-pass filtering of the total postsynaptic current at 1 Hz. Filtering at 1 Hz provided realistic extractions of the data without significant distortions in the time course or magnitude of the graded postsynaptic responses (comparisons were made with filtering at 3, 5, and 10 Hz) and eliminated all components of spike-mediated postsynaptic signals. Changes in Ca fluorescence ($\Delta F/F$) were measured in the main neurite and synaptic contact region corresponding to sites *1* and *4* of Figure 1*B*. $\Delta F/F$ was smoothed over seven points by an Origin 6.1 standard function, Adjacent Averaging, which calculates the smoothed value at index *i* as the average of the data points in the interval $[i-(n-1)/2, i+(n-1)/2]$, inclusive. *B*, Superimposed time courses of average graded postsynaptic response (*gIPSC*) and average Ca fluorescence signal ($\Delta F/F$) in the synaptic contact region under control conditions and in the presence of internal EGTA. Data are from *A*.

Photo-release of caged Ca^{2+} (NP-EGTA) profoundly alters the time course of depolarization-induced synaptic plasticity

To assess more directly the role of increases in background $[Ca^{2+}]_i$ in graded synaptic transmission and modulation in spike-mediated transmission, we used photo-induced release of caged Ca^{2+}. In these experiments (Figs. 8–10) and in subsequent experiments involving photo-release of caged Ca^{2+} chelator (Fig. 11), our releasing light flash produced a spot of ~60 μm in diameter, which we centered over the synaptic contact region of the heart interneurons. Ca fluorescence signals were recorded from the main neurite and from two concentric regions, one corresponding to the entire zone of photo-release (see Materials and Methods) and the other to the very center of this zone. Injection of NP-EGTA led to a strong reduction in Ca fluorescence signals produced by step depolarizations. This reduction is consistent with the known ability of NP-EGTA to act as an effective Ca^{2+} chelator with a nominal K_d of 80 nM (to be compared with a nominal K_d of 185 nM for Calcium Orange). In successful photo-release experiments, light flashes of 800 msec caused noticeable effects on synaptic transmission before the end of the flash (Figs. 8–10). For a period extending from the beginning of the flash to ~500 msec after the flash, we were unable to record a Ca fluorescence signal because of saturation of our camera; thereafter a clear Ca signal was recorded in each case.

In our first experiments ($n = 7$), we elicited simulated bursts superimposed on a flat but relatively depolarized (−45 to −40 mV) baseline potential (Fig. 8). In the absence of a light flash, we observed the expected stochastically varying postsynaptic responses. Photo-release of caged Ca^{2+} caused an increase in both the spike-mediated postsynaptic responses and graded transmission. These effects started before the end of the light flash and peaked in amplitude after the light flash. These results show that changes in background Ca^{2+} in the synaptic contact region induced by photo-release of caged Ca^{2+} can substitute for depolarization in mediating both graded synaptic transmission and modulation of spike-mediated transmission.

In subsequent experiments ($n = 4$), we elicited simulated bursts superimposed on a step depolarization from a hyperpolarized level (−70 to −60 mV). In the absence of a light flash, we observed increases in the spike-mediated postsynaptic responses associated with the step depolarization. Photo-release of caged Ca^{2+} caused an increase in both the spike-mediated postsynaptic responses and graded transmission. These effects started before the end of the light flash. In the experiment of Figure 9, the light flash was applied relatively late during the depolarized step and both spike-mediated and graded responses peaked near the end of the flash. In the experiment of Figure 10, the light flash was applied both late and early during the depolarized step, and in each case both spike-mediated and graded responses peaked during the flash. Comparison of the time courses of spike-mediated synaptic modulation under control conditions and during photo-release of caged Ca^{2+} indicates that the released Ca^{2+} profoundly alters the time course of depolarization-induced modulation.

Photo-release of caged Ca^{2+} chelator Diazo-2 profoundly alters the time course of depolarization-induced synaptic modulation

To test further the role of increases in background Ca^{2+} in graded synaptic transmission and modulation in spike-mediated transmission caused by step depolarizations, we used photo-release of caged Ca^{2+} chelator Diazo-2. Injection of Diazo-2 led to a slight reduction in Ca fluorescence signals produced by step depolarizations. This reduction is consistent with the known ability of Diazo-2 to act as a weak Ca^{2+} chelator with a nominal K_d of 2.2 μM (to be compared with a nominal K_d of 185 nM for Calcium Orange). In successful photo-release experiments (n = 23), light flashes of 800 msec caused noticeable effects on synaptic transmission before the end of the flash (Fig. 11). For a period extending from the beginning of the flash to ~500 msec after the flash, we were unable to record a Ca fluorescence signal because of saturation of our camera; thereafter a reduced Ca signal was recorded in each case. The released chelator has a nominal K_d of 80 nM. In these experiments, we elicited simulated bursts superimposed on a step depolarization from a hyperpolarized level (approximately −70 mV) (Fig. 11).

For 10 of 23 of these experiments (data not shown), in the absence of a light flash, we observed greatly reduced graded synaptic transmission, greatly reduced or eliminated spike-mediated synaptic transmission, and greatly reduced Ca fluorescence signals associated with the step depolarizations. The first photo-release of caged Ca^{2+} chelator eliminated all graded synaptic transmission and further reduced spike-mediated synaptic transmission. We assume that in these experiments the concentration of Diazo-2 in the cell was sufficient to buffer all internal Ca^{2+} involved in synaptic transmission and its modulation.

For 13 of 23 of these experiments, in the absence of a light flash, we observed the expected graded synaptic transmission, increases in the spike-mediated postsynaptic responses, and strong Ca fluorescence signal associated with the step depolarization. The first photo-release of caged Ca^{2+} chelator caused a precipitous decline in graded transmission, which started before the end of the light flash. Thereafter graded transmission was greatly suppressed (to no more than 5% of the preflash level), and Ca fluorescence signals were also reduced for the duration of the experiment. The effects of photo-release of caged Ca^{2+} chelator on plasticity of spike-mediated postsynaptic responses were small and transient by comparison. During the light flashes, the time course of synaptic plasticity was delayed. The maximal amplitude reached by the spike-mediated postsynaptic responses during the simulated burst was little affected, however, by the photo-release of the chelator. A subsequent control simulated burst after two chelator photo-releases displayed a normal time course for modulation of spike-mediated synaptic responses, but a reduced Ca fluorescence signal and little or no graded transmission. These results show that the released chelator can compete better for the Ca^{2+} that mediates graded synaptic release than for the Ca^{2+} that mediates and modulates spike-mediated synaptic release.

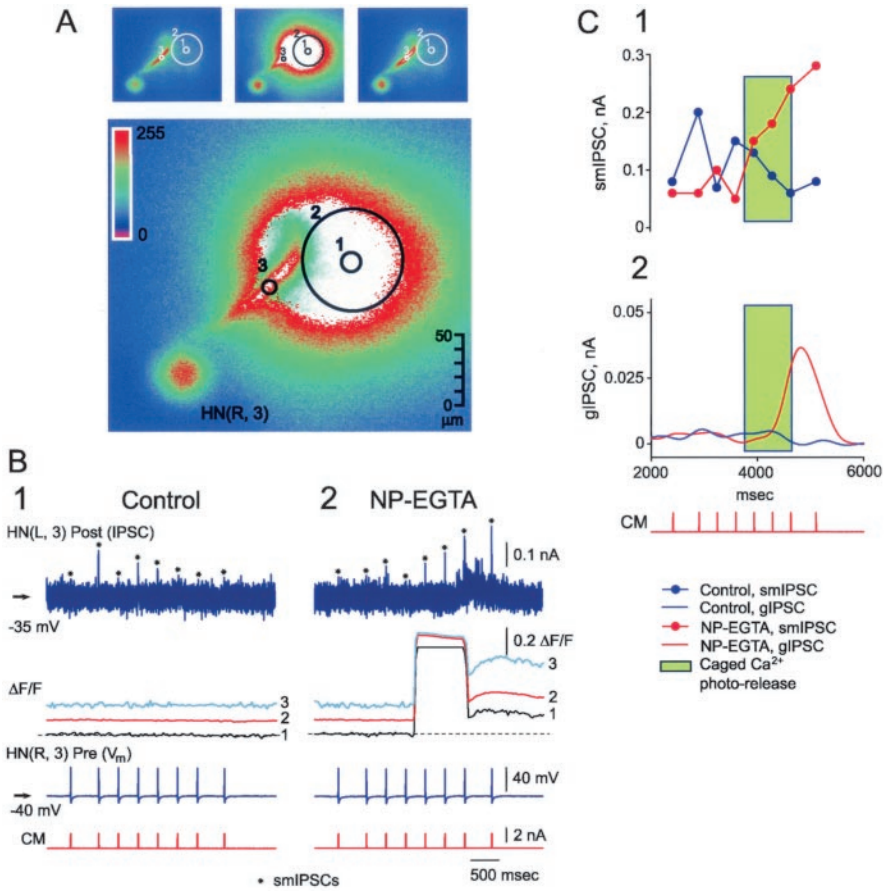

Figure 8. Photo-release of caged Ca^{2+} elicits graded transmission and enhances spike-mediated transmission when spikes are evoked from a steady holding potential. *A*, Ca fluorescence images of the presynaptic cell before, during, and after photo-release of caged Ca^{2+} (*top insets* from *left* to *right*). The *major panel* shows a combination of the before and during image at a larger scale. The *circles* show zones in which Ca fluorescence was monitored; the *circle* labeled *1* corresponds to the center of the releasing light beam, the *circle* labeled *2* shows the zone of photo-release as determined by the photo-release of caged fluorescein in the absence of a ganglion preparation, and the *circle* labeled *3* is in the main neurite. In all photo-release experiments, similar monitoring and release zones were used. *B*, Synaptic transmission in the absence (*1, Control*) and during photo-release of caged Ca^{2+} (*2, NP-EGTA*) in the same preparation. *C*, Plots of the time course of spike-mediated (*1, smIPSC*) and graded synaptic transmission (*2, gIPSC*) in the absence (*blue lines*) and during photo-release of caged Ca^{2+} (*red lines*). The *green bar* shows the duration of the releasing light flash.

Discussion

During their normal rhythmic activity, oscillator heart interneurons show cycle-by-cycle waxing and waning in the synaptic strength of their mutually inhibitory synapses (Thompson and Stent, 1976; Olsen and Calabrese, 1996). Synaptic transmission between these interneurons consists of both spike-mediated and graded components. Spike-mediated synaptic strength depends on the membrane potential baseline from which a presynaptic spike arises and not on previous spike activity; at a given baseline potential, postsynaptic responses are nearly constant over a large spike-frequency range (0.1–50 Hz) (Nicholls and Wallace, 1978a). Quantal analysis has shown that this effect of presynaptic baseline membrane potential is likely caused by modulation of release (Nicholls and Wallace, 1978b). The graded synaptic trans-

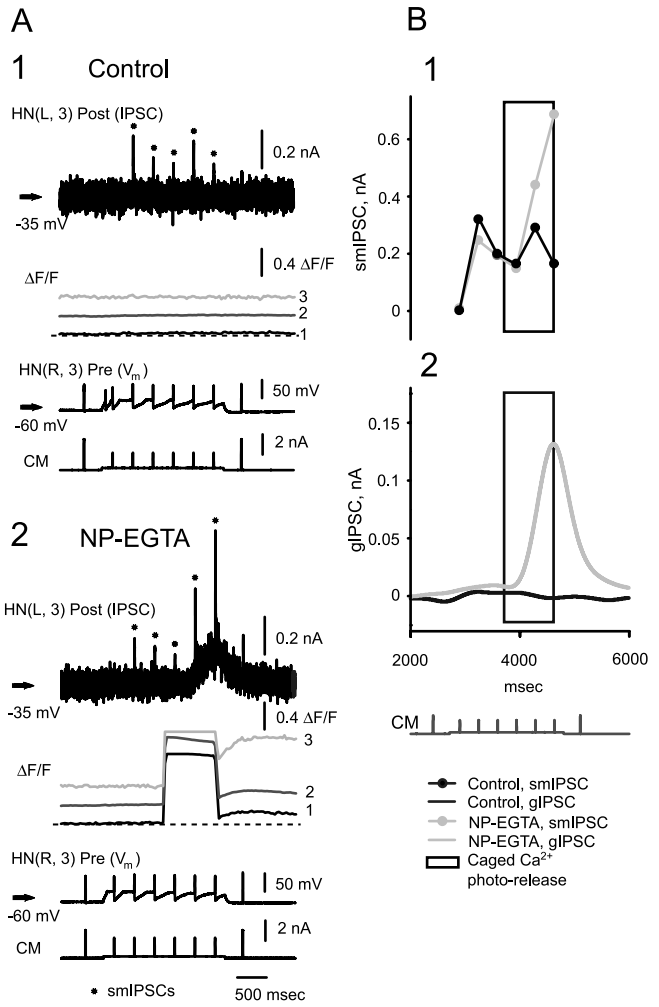

Figure 9. Photo-release of caged Ca^{2+} elicits graded transmission and enhances spike-mediated transmission by spikes superimposed on a step depolarization (simulated burst protocol). *A*, Synaptic transmission in the absence (*1, Control*) and during photo-release of caged Ca^{2+} (*2, NP-EGTA*) in the same preparation. *B*, Plots of the time course of spike-mediated (*1, smIPSC*) and graded synaptic transmission (*2, gIPSC*) in the absence (*black lines*) and during photo-release of caged Ca^{2+} (*gray lines*). The *white bar* shows the duration of the releasing light flash. Detectable smIPSCs elicited by the brief current pulses are indicated by *asterisks* (*A*). The first spike elicited by a current pulse during the step in *A1* and *A2* did not result in a detectable smIPSC; thus a zero value appears in the plots of *B1* where all responses to spikes elicited by pulses during the current step are plotted. The step depolarization itself elicited a spike in the control experiment (*A1*), but it elicited no detectable smIPSC response and was not plotted (*B1*).

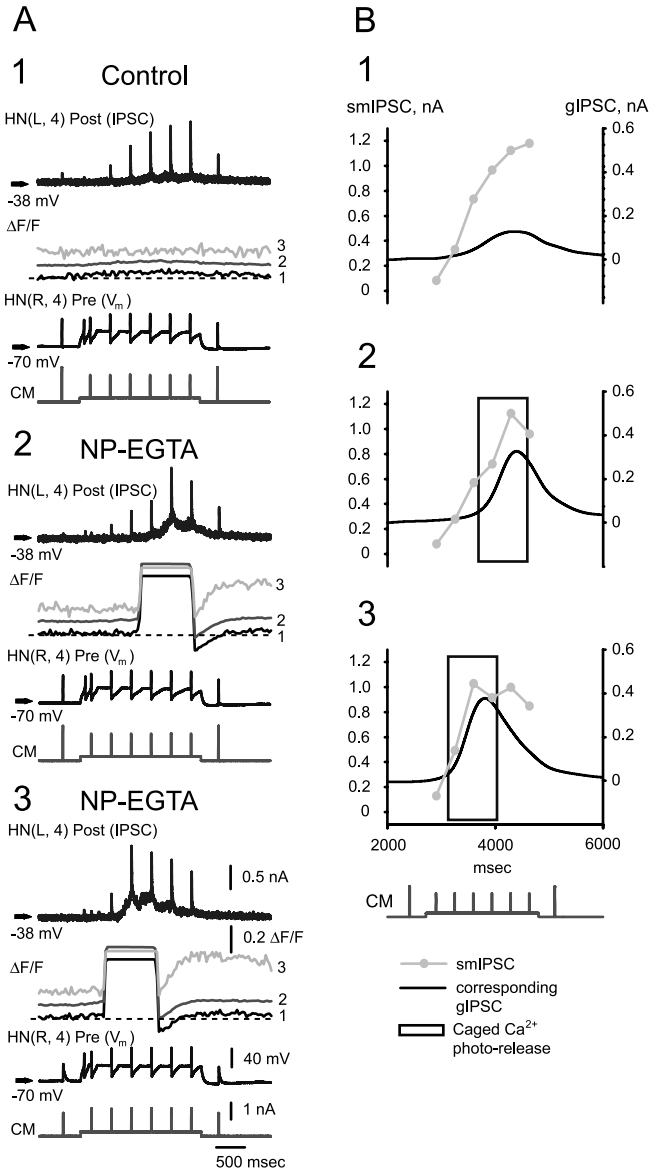

Figure 10. Photo-release of caged Ca^{2+} elicits graded transmission and enhances spike-mediated transmission by spikes superimposed on a step depolarization (simulated burst protocol). *A*, Synaptic transmission in the absence (*1, Control*) and during photo-release of caged Ca^{2+} (*2, 3, NP-EGTA*) in the same preparation. *B*, Plots of the time course of spike-mediated (*smIPSC*, *gray lines*) and graded synaptic transmission (*gIPSC*, *black lines*) in the absence (*1, Control*) and during two subsequent photo-releases of caged Ca^{2+} (*2, 3, NP-EGTA*). The *white bars* show the duration of the releasing light flash. Only the smIPSCs elicited by the brief current pulses during the depolarizing step are plotted. Plots correspond to *panels 1–3* in *A*.

mission depends on two low-threshold Ca^{2+} currents: one rapidly inactivating (I_{CaF}) and the other slowly inactivating (I_{CaS}) (Angstadt and Calabrese, 1991). Ca imaging experiments indicate that these low-threshold currents are widespread in the neurons and that they contribute to neuron-wide changes in internal background Ca^{2+} concentration (Ivanov and Calabrese, 2000). During normal rhythmic activity, background Ca^{2+} concentration oscillates, and thus graded synaptic transmission waxes and wanes as the neurons move from the depolarized to the inhibited phases of their activity.

In this study, we sought to determine whether changes in presynaptic background Ca^{2+} could account for the modulation of spike-mediated transmitter release by membrane potential and to define further the relationship of spike-mediated and graded synaptic transmission. We showed that the amplitude of spike-mediated postsynaptic responses correlates with the background concentration of Ca^{2+} recorded in the presynaptic cell. Furthermore, we showed that the modulation of spike-mediated transmission is independent of previous spike activity. During step changes in membrane potential, the time course of changes in spike-mediated transmission lags behind the time course of Ca^{2+} concentration changes in the synaptic contact region. In contrast, graded transmission follows the time course of Ca^{2+} concentration changes quite well. Delaying the time course of background Ca^{2+} buildup with internal EGTA delayed the time course of both graded transmission and the modulation of spike-mediated transmission and brought background Ca^{2+} buildup, graded transmission, and the modulation of spike-mediated

transmission into close register. With internal EGTA, there was a strong linear dependence of the amplitude of spike-mediated synaptic responses on the changes in Ca^{2+} concentration recorded in the synaptic contact region. Photo-release of caged Ca^{2+} augmented spike-mediated responses and evoked apparent graded transmission. Photo-release of caged Ca^{2+} chelator transiently delayed the buildup of spike-mediated responses associated with step depolarizations and strongly reduced graded synaptic transmission and Ca fluorescence signals for the duration of our experiments.

The role of residual or background Ca^{2+} in short-term synaptic enhancement

Current views of the mechanism of synaptic release involve a secretory trigger or calcium-binding sites that are closely associated with primed and docked vesicles. For spike-mediated (synchronous) synaptic transmission, the secretory trigger appears to be synaptotagmin 1 and is associated with synaptic vesicle membranes (Sugita et al., 2002). This sensor is thought to have relatively low affinity and fast binding dynamics for Ca^{2+}. Other synaptotagmins may also act as secretory triggers; e.g., synaptotagmin 7, which is associated with the presynaptic plasma membrane, has relatively high Ca^{2+} affinity and slow dynamics and appears to subserve asynchronous release (Sudhoff, 2002). At the release sites for spike-mediated transmission, high-threshold Ca channels are thought to be closely associated with a low-affinity secretory trigger, and Ca^{2+} entering through these channels during action potentials produces restricted Ca^{2+} domains that trigger release (Augustine et al., 1992; Stanley, 1993, 1997; Llinas et al., 1995; Neher, 1998). Augustine (2001) has coined the term nanodomains for the Ca^{2+} around a single channel that triggers the release of a single vesicle. Various forms of short-term synaptic enhancement have been thought to arise from residual Ca^{2+}, left after an action potential, that can bind to sites on the secretory trigger and thus augment the effects of Ca^{2+} entry from ensuing action potentials (Katz and Miledi, 1968; Magleby, 1979; Magleby and Zengel, 1982; Zengel and Magleby, 1982; Zucker, 1989). However, more recent studies of synaptic facilitation (Swandulla et al., 1991; Yamada and Zucker, 1992; Delaney and Tank, 1994; Kamiya and Zucker, 1994; Regehr et al., 1994; Atluri and Regehr, 1996; Zucker, 1999; Tang et al., 2000; Zucker and Regehr, 2002) have pointed to a high-affinity facilitation site for Ca^{2+} binding that may be spatially removed from the secretory trigger so that the Ca^{2+} in microdomains near the secretory trigger has restricted access to the facilitation site. Binding of Ca^{2+} at this facilitation site somehow readies vesicles for release, thus causing facilitation. Alternatively, the facilitation binding site may be a mobile Ca^{2+} buffer that is saturated by buildup of residual Ca^{2+}. Saturation of this buffer makes background Ca^{2+} available to the secretory trigger (Neher, 1998; Rozov et al., 2001).

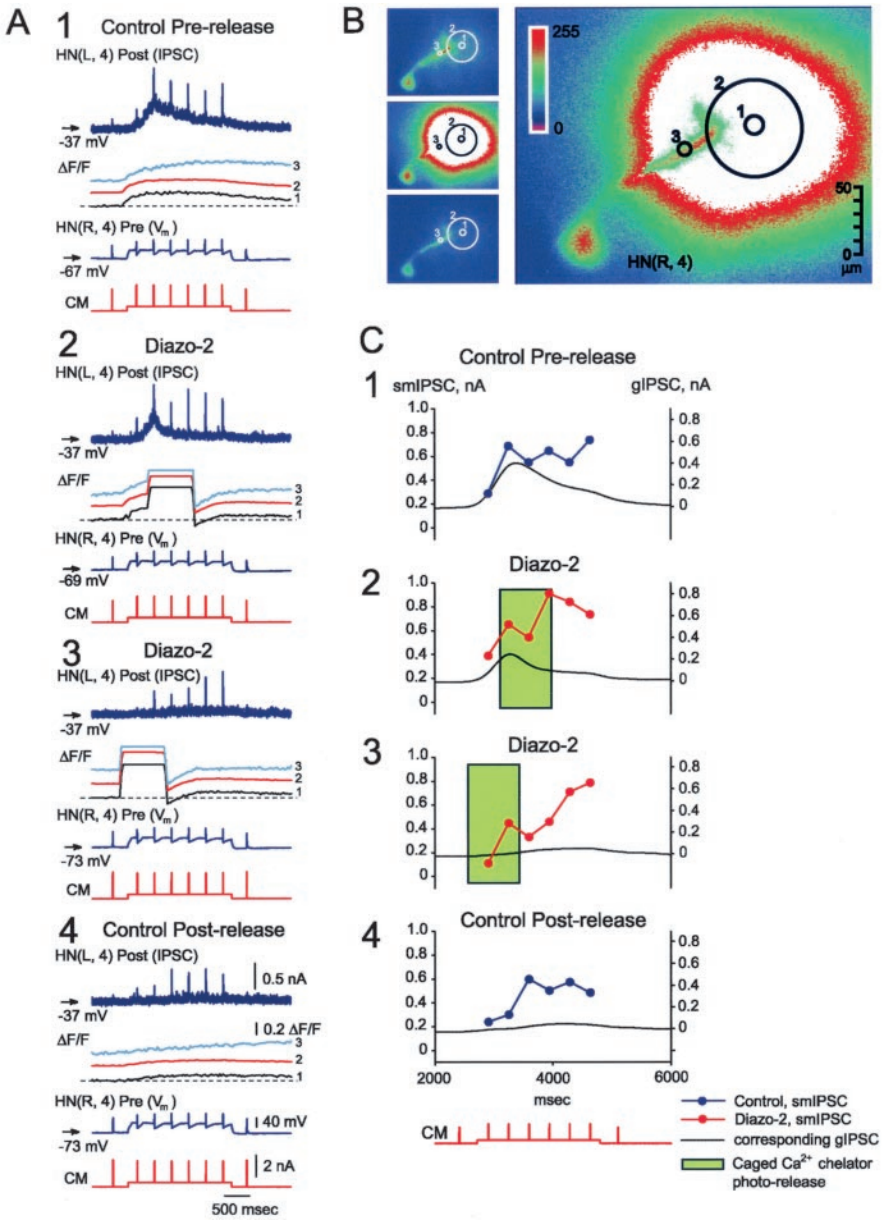

Figure 11. Photo-release of caged Ca^{2+} chelator suppresses graded transmission and alters the time course of plasticity in spike-mediated transmission by spikes superimposed on a step depolarization (simulated burst protocol). *A*, Synaptic transmission in the absence (*1, 4, Control Pre-release* and *Control Post-release*, respectively) and during two subsequent photo-releases of caged Ca^{2+} chelator (*2, 3, Diazo-2*) in the same preparation. *B*, Ca fluorescence images of the presynaptic cell before, during, and after photo-release of caged Ca^{2+} (*left insets* from *top* to *bottom* corresponding to the photo-release shown in *A2*). The *major panel* shows a combination of the before and during image at a larger scale. The *circles* show zones in which Ca fluorescence was monitored; the *circle* labeled *1* corresponds to the center of the releasing light beam, the *circle* labeled *2* shows the zone of photo-release as determined by the photo-release of caged fluorescein in the absence of a ganglion preparation, and the *circle* labeled *3* is in the main neurite. *C*, Plots of the time course of spike-mediated (*smIPSP*, *blue* and *red lines* for control and photo-release experiments, respectively) and graded synaptic transmission (*gIPSP*, *black lines*) in the absence (*1, Control Pre-release*; *4, Control Post-release*) and during two subsequent photo-releases of caged Ca^{2+} chelator (*2, 3, Diazo-2*). The *green bars* show the duration of the releasing light flash. Only the smIPSCs elicited by the brief current pulses during the depolarizing step are connected by *lines*. Plots correspond to *panels 1–4* of *A*.

Modulation of spike-mediated synaptic strength and control of graded synaptic transmission in leech heart interneurons: the role of background Ca^{2+}

Our previous work has indicated that two types of low-threshold Ca channels, one rapidly (I_{CaF}) and one slowly (I_{CaS}) inactivating, are widely distributed throughout heart interneurons; these gate graded synaptic transmission (Angstadt and Calabrese, 1991; Lu et al., 1997; Ivanov and Calabrese, 2000). The Ca^{2+} concentration changes that we record with our current methods appear to depend on Ca^{2+} entry through these low-threshold channels (Ivanov and Calabrese, 2000). There are also less well characterized high-threshold Ca channels of unknown location that apparently gate spike-mediated synaptic transmission (Simon et al., 1994; Lu et al., 1997). Ca imaging in other invertebrate neurons has demonstrated Ca^{2+} entry at restricted sites with high-threshold activation (Kloppenburg et al., 2000).

Our results suggest that the release sites for spike-mediated transmission in leech heart interneurons may be conventional, with high-threshold Ca channels closely associated with a low-affinity secretory trigger. The synaptic modulation that we observed here, however, appears to involve a high-affinity sensor that is acted on by background Ca^{2+} arising from low-threshold Ca channels that are widely dispersed throughout the neuritic processes of the cell. In contrast, in most models of enhancement, the Ca^{2+} that enhances release enters by high-threshold channels that are thought to be restricted to release sites and only activated by spike activity. Thus we prefer the term background Ca^{2+} to describe our results rather than residual Ca^{2+}, which has been defined as resulting from spike activity.

Background Ca^{2+} also appears to control graded synaptic transmission in heart interneurons. More tonic forms of release, such as from sensory cells, involve microdomains of Ca^{2+} from several channels (Augustine, 2001), and if the affinity of the secretory trigger is higher than previously thought, as suggested by experiments in the calyx of Held synapses (Schneggenburger and Neher, 2000), then the release machinery need not be in close association with Ca channels. Our observations on graded release are consistent with such a view; Ca^{2+} entering through low-threshold channels in these interneurons then may increase background Ca^{2+} to a sufficiently high level that release is mediated at sites with no closely associated Ca channels (sites specialized for graded transmission) and indeed even at sites with associated high-threshold channels (sites specialized for spike-mediated transmission).

Functional implications of the modulation of spike-mediated transmission by presynaptic background Ca^{2+} in leech heart interneurons

The pairs of heart interneurons studied here make strong mutually inhibitory synaptic connections to form half-center oscillators that under normal conditions produce continuous alternating bursting (period 6–10 sec) (Calabrese et al., 1995). The dependence of spike-mediated transmission on background Ca^{2+} levels in the neuron endows the heart interneurons with the ability to adjust synaptic strength in a continuous manner during rhythmic activity. The continuous modulation of synaptic strength appears to be important in determining the burst structure of the oscillator heart interneurons (Hill et al., 2001). Moreover, the modulation of spike-mediated transmission by background Ca^{2+} provides a mechanism to assure reciprocity between the two interneurons of a half-center oscillator. The low-threshold Ca currents that contribute to background Ca^{2+} in the heart interneurons also are critical in determining the burst activity. I_{CaS} in particular controls the strength and duration of the burst phase (Hill et al., 2001). Synaptic inhibition plays an important role in determining the amount of I_{CaS} available during the next ensuing burst, because the associated hyperpolarization removes inactivation from I_{CaS} after a burst. Thus strong synaptic inhibition from one interneuron will produce a strong I_{CaS} in the subsequent burst of the inhibited neuron. The resultant increase in background Ca^{2+} will thus ensure strong spike-mediated and graded inhibition of the opposite interneuron.

Wider implications of modulation of synaptic strength by background Ca^{2+}

Activity-dependent changes in background Ca^{2+} concentration have been implicated in the homeostatic regulation of intrinsic membrane currents and potentially synaptic strength (Turrigiano, 1999). Our findings presented here indicate that these changes in presynaptic background Ca^{2+} concentration also regulate synaptic transmission in an immediate way to modulate synaptic strength cycle by cycle in rhythmically active networks. Continuous activity-dependent modulation of synaptic strength of this kind seems particularly well suited to rhythmically active neuronal networks because it provides an activity-dependent mechanism on which exogenous neuromodulators can act.

References

Adams SR, Tsien RY (1993) Controlling cell chemistry with caged compounds. Annu Rev Physiol 55:755–784.

Angstadt JD, Calabrese RL (1991) Calcium currents and graded synaptic transmission between heart interneurons of the leech. J Neurosci 11:746–759.

Atluri PP, Regehr WG (1996) Determinants of the time course of facilitation at the granule cell to Purkinje cell synapse. J Neurosci 16:5661–5671.

Augustine GJ (2001) How does calcium trigger neurotransmitter release? Curr Opin Neurobiol 11:320–326.

Augustine GJ, Adler EM, Charlton MP, Hans M, Swandulla D, Zipser K (1992) Presynaptic calcium signals during neurotransmitter release: detection with fluorescent indicators and other calcium chelators. J Physiol (Paris) 86:129–134.

Blundon JA, Wright SN, Brodwick MS, Bittner GD (1993) Residual free calcium is not responsible for facilitation of neurotransmitter release. Proc Natl Acad Sci USA 90:9388–9392.

Calabrese RL, Nadim F, Olsen ØH (1995) Heartbeat control in the medicinal leech: a model system for understanding the origin, coordination, and modulation of rhythmic motor pattern. J Neurobiol 27:390–402.

Delaney KR (2000) Uncaging calcium in neurons. In: Imaging neurons. A laboratory manual (Yuste R, Lanni F, Konnerth A, eds), pp 1–26. Cold Spring Harbor, NY: Cold Spring Harbor Laboratory.

Delaney KR, Tank DW (1994) A quantitative measurement of the dependence of short-term synaptic enhancement on presynaptic residual calcium. J Neurosci 14:5885–5902.

Eberhard M, Erne P (1991) Calcium binding to fluorescent calcium indicators: Calcium Green, Calcium Orange and Calcium Crimson. Biochem Biophys Res Commun 180:209–215.

Ellis–Davies GCR, Kaplan JH (1994) Nitrophenyl-EGTA, a photolabile chelator that selectively binds Ca^{2+} with high affinity and releases it rapidly upon photolysis. Proc Natl Acad Sci USA 91:187–191.

Grynkiewicz G, Poenie M, Tsien RY (1985) A new generation of Ca^{2+} indicators with greatly improved fluorescence properties. J Biol Chem 260:3440–3450.

Haugland RP (2002) Handbook of fluorescent probes and research chemicals, Ed 9. Eugene, OR: Molecular Probes.

Hill AAV, Lu J, Masino MA, Olsen OH, Calabrese RL (2001) A model of a segmental oscillator in the leech heartbeat neuronal network. J Comput Neurosci 10:281–302.

Ivanov AI, Calabrese RL (2000) Intracellular Ca^{2+} dynamics during spontaneous and evoked activity of leech heart interneurons: low-threshold Ca currents and graded synaptic transmission. J Neurosci 20:4930–4943.

Jiang X-Y, Abrams TW (1998) Use-dependent decline of paired-pulse facil-

itation at *Aplysia* sensory neuron synapses suggests a distinct vesicle pool or release mechanism. J Neurosci 18:10310–10319.
Kamiya H, Zucker RS (1994) Residual Ca^{2+} and short-term synaptic plasticity. Nature 371:603–606.
Katz B, Miledi R (1968) The role of calcium in neuromuscular facilitation. J Physiol (Lond) 195:481–492.
Kloppenburg P, Zipfel WR, Webb WW, Harris-Warrick RM (2000) Highly localized Ca^{2+} accumulation revealed by multiphoton microscopy in an identified motoneuron and its modulation by dopamine. J Neurosci 20:2523–2533.
Llinás R, Sugimori M, Silver RB (1995) The concept of calcium concentration microdomain in synaptic transmission. Neuropharmacology 34:1443–1451.
Lu J, Dalton IVJF, Stokes DR, Calabrese RL (1997) Functional role of Ca^{2+} currents in graded and spike-mediated synaptic transmission between leech heart interneurons. J Neurophysiol 77:1779–1794.
Magleby KL (1979) Facilitation, augmentation, and potentiation of transmitter release. Prog Brain Res 49:175–182.
Magleby KL, Zengel JE (1982) A quantitative description of stimulation-induced changes in transmitter release at the frog neuromuscular junction. J Gen Physiol 80:613–638.
Nadim F, Manor Y, Kopell N, Marder E (1999) Synaptic depression creates a switch that controls the frequency of an oscillatory circuit. Proc Natl Acad Sci USA 96:8206–8211.
Neher E (1998) Vesicle pools and Ca^{2+} microdomains: new tools for understanding their roles in neurotransmitter release. Neuron 20:389–399.
Nerbonne JM (1996) Caged compounds: tools for illuminating neuronal responses and connections. Curr Opin Neurobiol 6:379–386.
Nicholls J, Wallace BG (1978a) Modulation of transmission at an inhibitory synapse in the central nervous system of the leech. J Physiol (Lond) 281:157–170.
Nicholls J, Wallace BG (1978b) Quantal analysis of transmitter release at an inhibitory synapse in the central nervous system of the leech. J Physiol (Lond) 281:171–185.
Nicholls JG, Baylor DA (1968) Specific modalities and receptive fields of sensory neurons in the central nervous system of the leech. J Neurophysiol 31:740–756.
Olsen ØH, Calabrese RL (1996) Activation of intrinsic and synaptic currents in leech heart interneurons by realistic waveforms. J Neurosci 16:4958–4970.
Parpura V, Haydon PG (1999) UV photolysis using a micromanipulated optical fiber to deliver UV energy directly to the sample. J Neurosci Methods 87:25–34.
Regehr WG, Delaney KR, Tank DW (1994) The role of presynaptic calcium in short-term enhancement at the hippocampal mossy fiber synapse. J Neurosci 14:523–537.
Rozov A, Burnashev N, Sakmann B, Neher E (2001) Transmitter release modulation by intracellular Ca^{2+} buffers in facilitating and depressing nerve terminals of pyramidal cells in layer 2/3 of the rat neocortex indicates a target cell-specific difference in presynaptic calcium dynamics. J Physiol (Lond) 531:807–826.
Schneggenburger R, Neher E (2000) Intracellular calcium dependence of transmitter release rates at a fast central synapse. Nature 406:889–893.
Simon TW, Schmidt J, Calabrese RL (1994) Modulation of high-threshold transmission between heart interneurons of the medicinal leech by FMRF-NH2. J Neurophysiol 71:454–466.
Stanley EF (1993) Single calcium channels and acetylcholine release at a presynaptic nerve terminal. Neuron 11:1007–1011.
Stanley EF (1997) The calcium channel and the organization of the presynaptic transmitter release face. Trends Neurosci 20:404–409.
Südhof TC (2002) Synaptotagmins: why so many? J Biol Chem 277:7629–7632.
Sugita S, Shin OH, Han W, Lao Y, Südhof TC (2002) Synaptotagmins form a hierarchy of exocytotic Ca(2+) sensors with distinct Ca(2+) affinities. EMBO J 21:270–280.
Swandulla D, Hans M, Zipser K, Augustine GJ (1991) Role of residual calcium in synaptic depression and posttetanic potentiation: fast and slow calcium signalling in nerve terminals. Neuron 7:915–926.
Tang Y, Schlumpberger T, Kim T, Lueker M, Zucker RS (2000) Effects of mobile buffers on facilitation: experimental and computational studies. Biophys J 78:2735–2751.
Thomas D, Tovey SC, Collins TJ, Bootman MD, Berridge MJ, Lipp P (2000) A comparison of fluorescent Ca^{2+} indicator properties and their use in measuring elementary and global Ca^{2+} signals. Cell Calcium 28:213–223.
Thompson WJ, Stent GS (1976) Neuronal control of heartbeat in the medicinal leech. III. Synaptic relations of heart interneurons. J Comp Physiol [A] 111:309–333.
Turrigiano GG (1999) Homeostatic plasticity in neuronal networks: the more things change, the more they stay the same. Trends Neurosci 22:221–227.
Wang SSH, Augustine GJ (1995) Confocal imaging and local photolysis of caged compounds: dual probes of synaptic function. Neuron 15:755–760.
Winslow JL, Duffy SN, Charlton MP (1994) Homosynaptic facilitation of transmitter release in crayfish is not affected by mobile calcium chelators: implications for the residual ionized calcium hypothesis from electrophysiological and computational analyses. J Neurophysiol 72:1769–1793.
Yamada WM, Zucker RS (1992) Time course of transmitter release calculated from simulations of a calcium diffusion model. Biophys J 61:671–682.
Zengel JE, Magleby KL (1982) Augmentation and facilitation of transmitter release. A quantitative description at the frog neuromuscular junction. J Gen Physiol 80:583–611.
Zucker RS (1989) Short-term synaptic plasticity. Annu Rev Neurosci 12:13–31.
Zucker RS (1999) Calcium and activity-dependent synaptic plasticity. Curr Opin Neurobiol 9:305–313.
Zucker RS, Regehr WG (2002) Short-term synaptic plasticity. Annu Rev Physiol 64:355–405.